Metamagnetism and Lifshitz transitions in models for heavy fermions

M. Bercx and F. F. Assaad

Institut für Theoretische Physik und Astrophysik, Universität Würzburg, Am Hubland, D-97074 Würzburg, Germany

(Received 8 June 2012; published 6 August 2012)

We investigate metamagnetic transitions in models for heavy fermions by considering the doped Kondo lattice model in two dimensions. Results are obtained within the framework of dynamical mean field and dynamical cluster approximations. Universal magnetization curves for different temperatures and Kondo couplings develop upon scaling with the lattice coherence temperature. Furthermore, the coupling of the local moments to the magnetic field is varied to take into account the different Landé factors of localized and itinerant electrons. The competition between the lattice coherence scale and the Zeeman energy scale allows for two interpretations of the metamagnetism in heavy fermions: Kondo breakdown or Lifshitz transitions. By tracking the single-particle residue through the transition, we can uniquely conclude in favor of the Lifshitz transition scenario. In this scenario, a quasiparticle band drops below the Fermi energy which leads to a change in topology of the Fermi surface.

DOI: 10.1103/PhysRevB.86.075108 PACS number(s): 71.27.+a, 75.30.Kz, 75.30.Mb, 71.10.Fd

I. INTRODUCTION

Kondo lattice systems are states of matter whose low-temperature macroscopic properties are dominated by strong correlations between Bloch fermion states and local spin moments. They can host various, sometimes competing orders and are therefore susceptible to tuning of external parameters. How the strongly entangled Kondo state evolves when competing mechanisms appear constitutes a vibrant area of research.[1–3] Prototypical heavy fermion materials are intermetallic compounds with the rare-earth elements Ce or Yb that deliver almost localized f electrons.

When an external magnetic field is applied to certain fermion systems, unexpected nonlinear behavior of the magnetization at a well defined field value enters the stage.[4,5] Equally, distinct anomalies of thermodynamic quantities and in transport measurements occur at the same magnetic field.[6,7] This phenomenon has been dubbed metamagnetism. At the critical field, the heavy electron Fermi surface changes its topology.[6,8–10] Recent experiments witness a pronounced, first-order metamagnetic transition (MMT) in the heavy-fermion paramagnet CeTiGe.[5] Metamagnetism has been known to occur in $CeRu_2Si_2$[4] and, amongst other fermionic systems, a pressure-tuned first-order MMT has been observed in bilayer ruthenates.[11]

The thermodynamic signatures of heavy fermion compounds have been related to a metamagnetic quantum critical endpoint of the Ising universality class.[12,13] The MMT in heavy fermion systems has been addressed by static mean-field (MF) studies[14,15]—presupposing a continuous transition—and by dynamical mean field theory (DMFT). The magnetization profile in Kondo systems has been shown to be closely related to the quasiparticle coherence.[16] Also, crystal field effects have been included in a DMFT study.[17] Apart from heavy fermion systems, the metamagnetism of itinerant electrons has been addressed by MF methods,[18] functional renormalization group,[19] and DMFT.[20]

Lifshitz transitions are quantum phase transitions which invoke a topological change of the Fermi surface.[21–23] Lifshitz transitions and Kondo breakdown scenarios have been investigated in fermionic large-N approaches.[24,25] Zeeman-driven Lifshitz transitions were shown to explain many anomalies in thermodynamic and transport measurements of certain heavy fermion metals.[26]

This study is motivated by the interplay of two competing energy scales, the lattice coherence scale and a magnetic Zeeman scale. By varying the magnitude of the Landé factors we can show that the metamagnetic transition occurs when both scales are comparable, thus allowing for interpretations based on Kondo breakdown or Lifshitz transitions. The single-particle residue is measured as a function of magnetic field throughout the MMT and is shown to be consistent with the picture of a coherent band dropping below the Fermi energy at the transition. We supplement our analysis by single-particle spectral data. Our results clearly point towards Lifshitz physics as the key player in the MMT in models of heavy fermions.

We draw this conclusion based on a dynamical cluster approximation (DCA) calculation of the Kondo lattice model with a Hirsch-Fye quantum Monte Carlo (HF-QMC) solver.

The paper is organized as follows. Section II introduces the model Hamiltonian and Sec. III reviews the DCA implementation. Sections IV and V contain the results of this study. We finish with a discussion (Sec. VI) and the conclusion (Sec. VII).

II. MODEL

The essential aspects of heavy fermion systems are captured by the Kondo lattice model (KLM).[27,28] The KLM is an effective low-energy model which is obtained upon integrating out the valence fluctuations of the f orbitals in the periodic Anderson model.[29,30] In particular, the model captures the crossover from independent magnetic impurities embedded in a metallic host to a coherent heavy fermion state. The KLM at half-filling has a unique spin singlet, insulating ground state[31] that is adiabatically connected to the trivial band insulator of the non interacting periodic Anderson model.[30] The weakly doped KLM exhibits a Fermi-liquid ground state.[32]

We investigate this model by means of DMFT and DCA[33,34] with a quantum Monte Carlo cluster solver. The cluster approximation is on spatial correlations which are essentially cut off by the cluster dimension. Temporal correlations that

drive the Kondo effect are fully accounted for in DMFT and its cluster extensions.

We study the KLM supplemented with Zeeman terms on the two-dimensional square lattice, $\mathcal{H} = \mathcal{H}_t + \mathcal{H}_J + \mathcal{H}_B$:

$$\mathcal{H} = -t \sum_{\langle i,j\rangle,\sigma} (c^\dagger_{i,\sigma} c_{j,\sigma} + \text{H.c.}) + J \sum_i \mathbf{S}^c_i \cdot \mathbf{S}^f_i - \mu_B B \sum_i \left(g_c S^c_{z,i} + g_f S^f_{z,i}\right). \quad (1)$$

The magnetic moments of itinerant (c) and local (f) orbitals along the direction of the applied field are given by $\mu^{c,f}_{z,i} = \mu_B g_{c,f} S^{c,f}_{z,i}$. The couplings g_c and g_f are understood as parameters. Physically, this is motivated by the pseudospin nature of $S^f_{z,i}$: the spin degree of freedom originates from a Kramer doublet and can take large values, which in turn renormalizes the g factor g_f.[20]

Drawing on the recently obtained phase diagram of the two-dimensional KLM[32,35,36] we concentrate on the paramagnetic side of the transition and consider a metallic state with the conduction band filling $n_c = 0.9$.

The lattice of impurities introduces the coherence scale T_{coh} as the natural energy scale.[37] The single-impurity Kondo scale, itself being the natural scale in a single-impurity model, is a local scale.[27]

Guidelines for these two scales in the KLM are provided by large-N calculations.[38] In the weak coupling limit ($J/W \ll 1$, W is the bandwidth) and at small deviation from half-filling ($1 - n_c \ll 1$), a scaling of $T_{\text{coh}} \propto T_K \propto W e^{-\rho_0(\epsilon_F)/J}$ is obtained [$\rho_0(\epsilon_F)$ is the free density of states at the Fermi level].

Two-dimensional Kondo systems are realized in surface alloys, e.g., in the heavy fermion compound $CePt_5$.[39,40] In the case that the distance to a continuous quantum critical point is large enough so that the zero-dimensional Kondo effect dominates over spatial fluctuations, one can expect that a similar scenario of competing energy scales applies to the three-dimensional case.

In the model [Eq. (1)] spin-orbit coupling is neglected, which would generally cause the g factor to be a tensor. Realistic modeling of heavy fermion materials requires a more sophisticated approach, capturing these material-specific features. Instead, the used model serves the purpose of describing the generic interplay between the magnetic Zeeman scale and the coherence scale of the Kondo system, which can lead either to the Kondo breakdown or the Lifshitz transition scenario.

III. METHOD

We use the Hirsch-Fye QMC technique to solve the KLM on small clusters that contain two orbitals (DMFT limit) and four orbitals, respectively. Cluster approximation schemes are particularly well designed to capture the Kondo physics since temporal correlations can be treated exactly. The approximation is on spatial correlations that are short ranged in the present situation. The DCA is a fully causal, nonperturbative method which is systematically improved by increasing the cluster sizes.[33,34] In the following, we outline our implementation for the KLM.

A static mean-field perspective can provide insight into the low-energy properties of the KLM.[41] It roots on the saddle-point approximation which is the exact solution of the $SU(N)$ KLM in the limit of $N = \infty$. However, it exhibits an unphysical phase transition instead of the Kondo crossover. Appropriate choices of the magnetic matrix elements that couple the impurity f orbitals to the external magnetic filed can recover the smooth Kondo crossover even in the large-N limit of the KLM with an external magnetic field term.[42]

In order to solve the KLM, we implement the following Hamiltonian:[16,43]

$$\mathcal{H} = \mathcal{H}_0 + \mathcal{H}_U - \frac{J}{4} \sum_i \left[\sum_\sigma c^\dagger_{i,\sigma} f_{i,\sigma} + f^\dagger_{i,\sigma} c_{i,\sigma} \right]^2. \quad (2)$$

Here, $\mathcal{H}_0 = \mathcal{H}_t + \mathcal{H}_B$ and the Hubbard term $\mathcal{H}_U = \frac{U_f}{2} \sum_i [\sum_\sigma n^f_{i\sigma} - 1]^2$ has been introduced. Local spin operators S^f_i are as usually mapped to auxiliary lattice fermions, $S^f_i = \frac{1}{2} \sum_{\alpha,\beta} f^\dagger_{i,\alpha} \sigma_{\alpha\beta} f_{i,\beta}$. Their single occupancy is guaranteed for $U_f \to \infty$ and, in this limit, the Hamiltonian (2) is equivalent to the KLM (1).

The discretization $\beta = M \Delta\tau$ on the interval $[0,\beta]$ gives the partition function $Z = Z_{\Delta\tau} + \mathcal{O}[(\Delta\tau)^2]$, with

$$Z_{\Delta\tau} = \text{Tr} \prod_{l=1}^{M} \left\{ \exp[-\Delta\tau \mathcal{H}_0] \int D[\lambda] \exp\left[-i\Delta\tau \sum_i \lambda_{li} \left(\sum_\sigma n^f_{i\sigma} - 1 \right) \right] \times \int D[\phi] \exp\left[-\Delta\tau J \sum_i \left(\phi^2_{li} - \phi_{li} \sum_\sigma (c^\dagger_{i,\sigma} f_{i,\sigma} + \text{H.c.}) \right) \right] \right\} = \int \text{D}[\lambda,\phi] \exp\left[-S_{\text{eff}}[\lambda,\phi] \right]. \quad (3)$$

In Eq. (3), the two successive Hubbard-Stratonovich (HS) transformations reduce the quartic fermion terms to quadratic terms. The integration measures $D[\lambda,\phi]$ denote integration over spatial and time indices of the fields and contain normalization factors.

The saddle point of the above defined action fulfills $\partial S_{\text{eff}}/\partial\phi_{li} = \partial S_{\text{eff}}/\partial\lambda_{li} = 0$. Static mean-field theory is obtained by dropping the τ dependence in the HS fields, and one can furthermore request the homogeneous solution: $\phi_{li} \equiv \phi_0, \lambda_{li} \equiv \lambda_0$. The saddle-point equations,

$$\phi_0 = \frac{1}{2N} \left\langle \sum_{i\sigma} c^\dagger_{i,\sigma} f_{i,\sigma} + \text{H.c.} \right\rangle_{\text{MF}}, \quad 1 = \frac{1}{N} \left\langle \sum_{i\sigma} n^f_{i,\sigma} \right\rangle_{\text{MF}}, \quad (4)$$

are then solved self-consistently. The respective mean-field results for total magnetization and quasiparticle residues are discussed in Sec. IV.

In order to go beyond mean field, a systematic $1/N$ expansion around the mean-field solution can be performed.[44] Instead, we integrate over all the field configurations through application of the HF-QMC algorithm. The trace in Eq. (3) can be carried out and expressed as a determinant of the Green's function matrix g_σ. Then, the partition function

$$Z_{\Delta\tau} = \int D[\lambda,\phi] \prod_\sigma \det\left[g_\sigma^{-1}\right] \tag{5}$$

is sampled stochastically. In the actual implementation, two discrete HS transformation are used.[43] The Green's function matrix is measured and updated according to the Hirsch-Fye algorithm.[45] During the simulation of Eq. (2), double occupancy of the f orbitals can be suppressed to the desired accuracy. We take $\Delta\tau = 0.25$ during the simulations. We have checked that smaller values of $\Delta\tau$ do not alter the results.

The cluster approximation amounts to considering the interaction terms of the Hamiltonian only on a subset $\mathcal{M}$ of the lattice with N_c sites, which naturally defines the extent to which spatial correlations are captured. We therefore solve the model

$$\mathcal{H} = \tilde{\mathcal{H}}_0 + J \sum_{R\in\mathcal{M}} \mathbf{S}_R^c \cdot \mathbf{S}_R^f, \tag{6}$$

by using the auxiliary Hamiltonian (2). $\tilde{\mathcal{H}}_0$ denotes the bath which is determined self-consistently.

The DCA is naturally described in momentum space since it relies on coarse graining of momentum space. Since the interaction part of the Hamiltonian is local, it is not affected by the coarse graining. The model Hamiltonian is solved on a finite cluster of N_c sites that is embedded in a bath of N sites ($N \gg N_c$). Since N is not a limiting factor one can work directly in the thermodynamic limit. Therefore, the DCA interpolates between two limiting cases: the DMFT ($N_c = 1$) and the finite lattice ($N_c = N$).

The DCA lattice self-energy is a step function in reciprocal space:

$$\begin{aligned} \Sigma_{\text{Latt}}^{\text{DCA}}(\mathbf{K},\omega) &= \frac{N_c}{N} \sum_{\tilde{\mathbf{k}}} \Sigma_{\text{Latt}}(\mathbf{K}+\tilde{\mathbf{k}},\omega), \\ \lim_{N_c\to N} \Sigma_{\text{Latt}}^{\text{DCA}}(\mathbf{K},\omega) &= \Sigma_{\text{Latt}}(\mathbf{K},\omega). \end{aligned} \tag{7}$$

The step size is $\Delta\mathbf{K} = 2\pi/N_c$, the cluster momenta $\mathbf{K}$ define the centers of N_c reciprocal cells, and $\tilde{\mathbf{k}}$ denotes the k points that lie within these cells. The DCA self-consistent scheme operates on the single-particle level of the self-energies and it demands that $\Sigma_{\text{Cluster}}^{\text{DCA}}(\mathbf{K},\omega) = \Sigma_{\text{Latt}}^{\text{DCA}}(\mathbf{K},\omega)$. The self-consistent equations are

$$\begin{aligned} \Sigma_{\text{Cluster}}^{\text{DCA}}(\mathbf{K},\omega) = {} & G_{\text{Latt,av.}}^{\text{DCA}}(\mathbf{K},\omega)^{-1} + \Sigma_{\text{Latt}}^{\text{DCA}}(\mathbf{K},\omega) \\ & - G_{\text{Cluster}}^{\text{DCA}}(\mathbf{K},\omega)^{-1}. \end{aligned} \tag{8}$$

Here, an effective bare Green function has been defined as

$$\mathcal{G}_{\text{Cluster}}^{\text{DCA}}(\mathbf{K},\omega)^{-1} = G_{\text{Latt,av.}}^{\text{DCA}}(\mathbf{K},\omega)^{-1} + \Sigma_{\text{Latt}}^{\text{DCA}}(\mathbf{K},\omega). \tag{9}$$

The DCA lattice averaged Green functions are coarse-grained averages over cell momenta:

$$G_{\text{Latt,av.}}^{\text{DCA}}(\mathbf{K},\omega) = \frac{N_c}{N} \sum_{\tilde{\mathbf{k}}} \frac{1}{\omega - \epsilon(\mathbf{K}+\tilde{\mathbf{k}}) + \mu - \Sigma_{\text{Latt}}^{\text{DCA}}(\mathbf{K},\omega)}. \tag{10}$$

The Green function $\mathcal{G}_{\text{Cluster}}^{\text{DCA}}(\mathbf{K},\omega)$ is the bare Green function that is the input for the cluster calculation. The cluster calculation yields the cluster Green functions $G_{\text{Cluster}}^{\text{DCA}}(\mathbf{K},\omega)$ that enter Eq. (8). Once the self-energy is converged, the DCA lattice Green function is computed:

$$G_{\text{Latt}}^{\text{DCA}}(\mathbf{k},\omega)^{-1} = \omega - \epsilon(\mathbf{k}) + \mu - \Sigma_{\text{Latt}}^{\text{DCA}}(M(\mathbf{k}),\omega). \tag{11}$$

The function $M:\mathbf{k}\to\mathbf{K}$ uniquely maps momenta to the reciprocal cells.

The required CPU time of the HF-QMC algorithm scales as $(\beta N_c)^3$.

IV. RESULTS

The magnetic field tunes the interacting Kondo system [Eq. (1)] from strong coupling at low fields to weak coupling at high fields, $B/T_{\text{coh}} \gg 1$. This limit is adiabatically connected to two copies of non interacting c electrons, spin split by the Zeeman energy, and fully polarized f moments. At low values of the magnetic field, the hybridized band is expected to shift in a rigid manner. At an intermediate energy scale, $B \sim T_{\text{coh}}$, two different scenarios are conceivable: (1) a breakdown of the Kondo effect itself at the relevant energy scale, or (2) a continuous transition that preserves the quasiparticles. In scenario (1), the quasiparticle itself is destroyed by the magnetic field. The single-particle residue quantifies the overlap of the interacting wave function with a bare conduction electron wave function. Therefore, the loss of quasiparticle coherence has to manifest itself as a sudden drop in this quantity for both both spin projections. In scenario (2), quasiparticles remain intact at the Fermi level. The spin-dependent Fermi surfaces undergo Lifshitz transitions which modify their topology. As shown below, data for the single-particle residue and single-particle spectral function across the MMT support scenario (2).

The mean-field solution, derived from the saddle-point of the $SU(N)$ KLM, can be seen as the best approximation in quadratic fermionic terms to the fully correlated model. Therefore, in the case that DMFT/DCA calculations support the notion of quasiparticles, the MF perspective is legitimate. The MF results are intended to complete the above described scenario of Lifshitz transitions.

The magnetization profile of a heavy fermion model system can serve directly as a measure of coherence. The plateau of the occupation number difference $m = \sum_\sigma \sigma(n_\sigma^c + n_\sigma^f)$ directly relates to the hybridization gap in the quasiparticle bands.[16] Its position is fixed to $x = 1 - n_c$ by the Luttinger sum rule. The physical magnetization $M = -\frac{\partial \mathcal{F}}{\partial B} = \sum_\sigma \sigma(g_c n_\sigma^c + g_f n_\sigma^f)$ does not generally display a plateau when the orbital couplings are not the same.

A. Data collapse $M(g_f/g_c, T/T_{\rm coh}, B/T_{\rm coh})$

For temperatures below the coherence scale $T_{\rm coh}$ quasiparticle bands are formed via coherent superposition of the screening clouds of the local spins. To verify that the coherence scale is the unique underlying scale a data collapse of DMFT and DCA data is carried out by scaling the magnetization with $T_{\rm coh}$. Because the plateau width of the occupation number is a measure of the hybridization gap, a good estimate of $T_{\rm coh}$ is obtained from the position of the second kink at $B = B_{\rm L2}$, determined by the intersections of linear fits at $\beta t = 100$ and $g_f/g_c = 1$. The scaling then becomes

$$M(g_f/g_c, T, B, J) \rightarrow M(g_f/g_c, T/T_{\rm coh}, B/T_{\rm coh}). \quad (12)$$

Effectively, the Kondo coupling J/t has disappeared as a parameter in M. The data collapse is evident, as shown in Fig. 1.

For all values of g_f/g_c the magnetization shows two pronounced kinks at $B = B_{\rm L1,2}$. The driving mechanism that shapes the magnetization is rooted in the competition of two energy scales: the dominant magnetic energy scale $g_f \mu_B B$ and the Kondo scale $T_{\rm coh}$. At the second kink both scales become comparable, such that $B_{\rm L2} \propto g_f^{-1}$. The position of the second kink in dependence of the coupling ratio is shown in Fig. 2, and the data are in good agreement with the above argument.

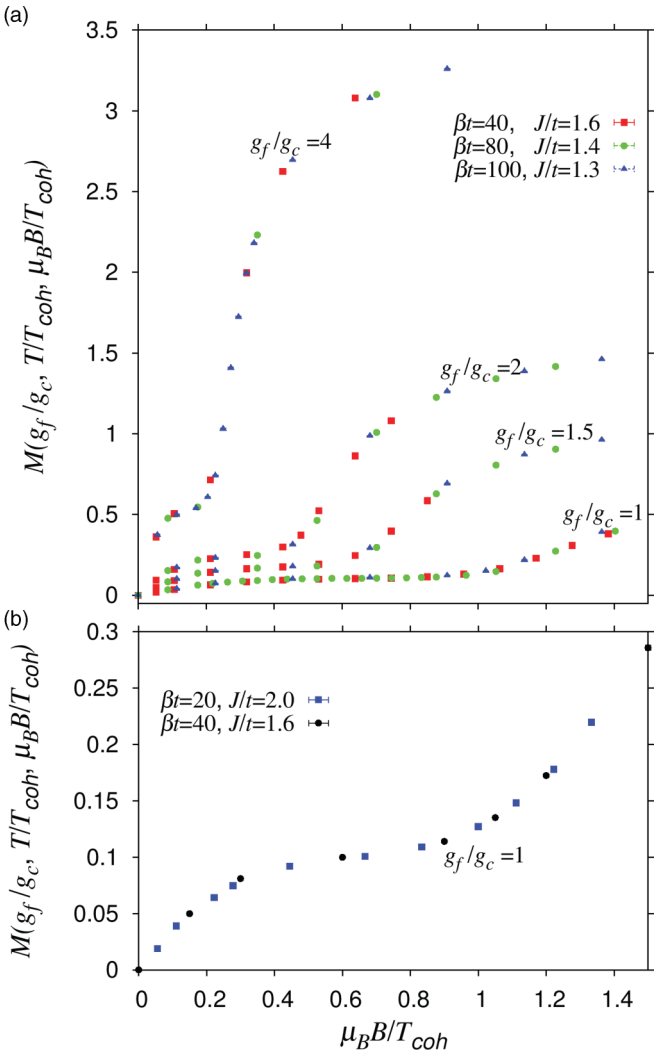

FIG. 1. (Color online) $T_{\rm coh}$-scaled magnetization $M(g_f/g_c, T/T_{\rm coh}, B/T_{\rm coh})$ for (a) two-orbital DMFT and (b) four-orbital DCA. The respective coherence temperatures are (a) $T_{\rm coh}(g_f/g_c = 1, J/t = 1.6) = 0.094t$, $T_{\rm coh}(g_f/g_c = 1, J/t = 1.4) = 0.057t$, and $T_{\rm coh}(g_f/g_c = 1, J/t = 1.3) = 0.044t$; (b) $T_{\rm coh}(g_f/g_c = 1, J/t = 1.6) = 0.10t$ and $T_{\rm coh}(g_f/g_c = 1, J/t = 2.0) = 0.18t$.

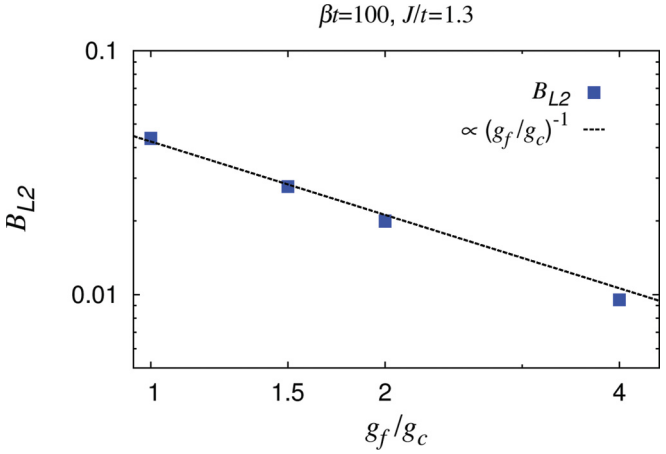

FIG. 2. (Color online) The magnetic field value of the second Lifshitz transition, $B_{\rm L2}(g_f/g_c)$, agrees well with $B_{\rm L2}(g_f/g_c) \propto (g_f/g_c)^{-1}$.

Increased Zeeman coupling to the local spins provokes the intermediate, plateaulike region to decrease and renders the increase at $B = B_{\rm L2}$ much steeper.

Static MF calculations succeed in reproducing the qualitative shape of M (Fig. 3). In the MF picture, the two kinks in the magnetization correspond to two Lifshitz transitions.

At this point, the data collapse of the magnetization can be compared to a scaling approach of the resistivity in a recent cluster DMFT (CDMFT) study of the Anderson lattice model close to half-filling of the conduction band, which equally reveals the lattice coherence temperature as the single underlying energy scale.[46]

Our calculated metamagnetic curves, as shown in Fig. 1, bear notable similarity with recent experimental data of the paramagnetic heavy-fermion system CeTiGe.[5] This is discussed in Sec. VI.

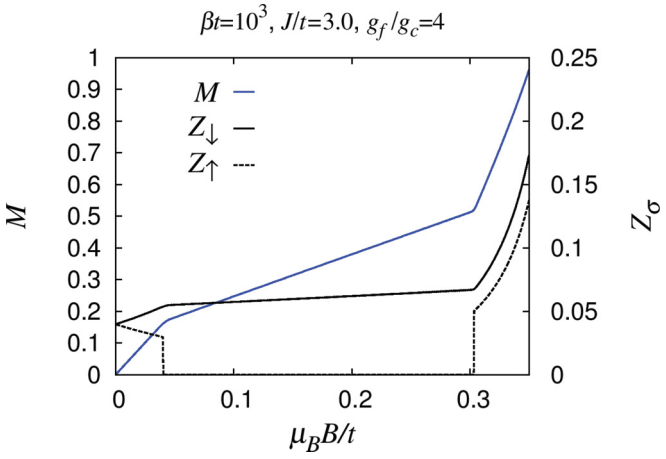

FIG. 3. (Color online) Static MF results for the magnetization M and single-particle residue Z_σ.

B. Single-particle quantities: residue Z_σ and spectral function $A_\sigma(\mathbf{k},\omega)$

The analysis of the single-particle quantities is based on the observation that the KLM has a Fermi-liquid ground state for the chosen value of conduction band filling, $n_c = 0.9$.,[32] and for zero external magnetic field. The calculations were performed for $J/t = 1.3$, $g_f/g_c = 4$, $\beta t = 100$, and $\beta t = 200$. For these parameters, we identify two Lifshitz transitions that occur at $\mu_B B_{L1}/t \approx 0.002$ and at $\mu_B B_{L2}/t \approx 0.01075$. The latter corresponds to the MMT.

A Fermi-liquid signature is the analyticity of the retarded self-energy $\Sigma(\mathbf{k},\omega)$ around the Fermi energy such that $\Sigma(\mathbf{k},\omega)$ allows for polynomial expansion. Then, the single-particle residue reads, expressed with the k-independent Matsubara self-energy $\Sigma_\sigma^{\mathrm{DMFT}}(i\omega_n)$,

$$\left[Z_\sigma^{\mathrm{DMFT}}\right]^{-1} = \lim_{T\to 0}\left[1 - \frac{\mathrm{Im}\Sigma_\sigma^{\mathrm{DMFT}}(\omega_n)}{\omega_n}\right]_{\omega_n=\pi T}. \quad (13)$$

The quantity $\mathrm{Im}\Sigma_\sigma^{\mathrm{DMFT}}(\omega_n)$ across the MMT at $B = B_{L2}$ is displayed in Fig. 4. Evidently, the imaginary part of the Matsubara self-energy is free of divergences for both spin projections at low frequencies ω_n. We take this as evidence for the continuous transition scenario.

The excitations are tracked by the single-particle spectral function

$$A_\sigma(\mathbf{k},\omega) = -\frac{1}{\pi}\mathrm{Im}G^\sigma_{\mathrm{Latt}}(\mathbf{k},\omega); \quad (14)$$

see Fig. 5. The analytic continuation from imaginary time-dependent QMC data has been performed with the stochastic maximum entropy method.[47]

The single-particle residues Z_σ at $\beta t = 100$ and $\beta t = 200$ across the MMT are shown in Fig. 6(b). $Z_\downarrow$ essentially follows the magnetization $M(B)$ [Fig. 6(a)]. $A_\downarrow(\mathbf{k},\omega)$ displays well defined quasiparticle weight across the MMT (Fig. 5) and hence accounts for a metallic state.

$Z_\uparrow$ vanishes for an intermediate magnetic field range, close to $B_{L1} < B < B_{L2}$. In this locked phase, no up-spin Fermi surface is present. At $B = B_{L2}$, a topological change of the Fermi surface occurs since one up-spin band crosses the Fermi

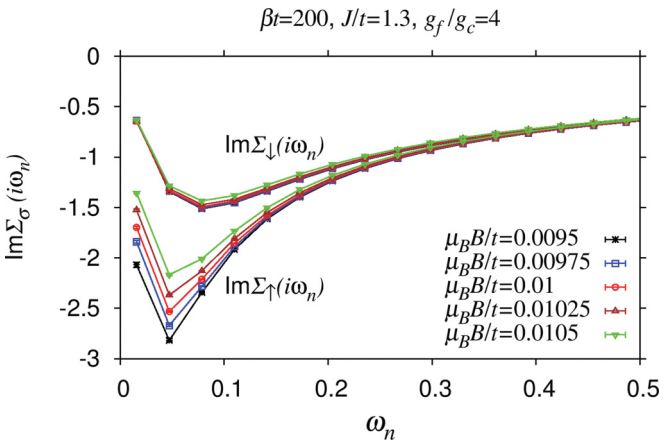

FIG. 4. (Color online) The imaginary part of Matsubara self-energies $\mathrm{Im}\Sigma^{\mathrm{DMFT}}_{\sigma=\downarrow,\uparrow}(i\omega_n)$ at values of the magnetic field close to $B = B_{L2}$.

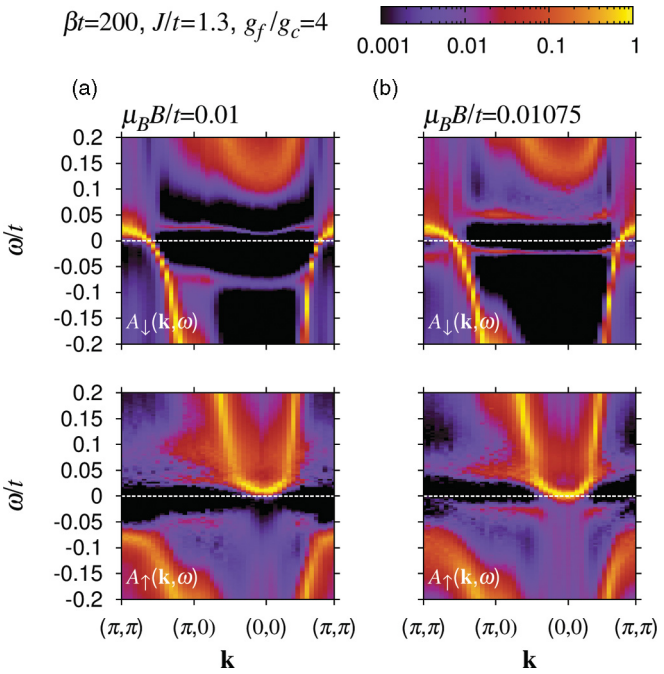

FIG. 5. (Color online) Single-particle spectral function $A_\sigma(\mathbf{k},\omega)$ across the MMT at the lowest temperature, $\beta t = 200$ (magnetic field values are indicated by arrows in Fig. 6). The narrow distribution of spectral weight close to the Fermi energy (dashed line) indicates that Kondo coherence remains across the MMT.

level at the gamma point, $(k_x,k_y) = (0,0)$. $A_\uparrow(\mathbf{k},\omega)$ shows a sharply defined quasiparticle band just below and at $B = B_{L2}$; see Figs. 5(a) and 5(b). The fact that the residue $Z_\uparrow$ does not vanish exactly at $B = B_{L2}$ can be related to the finite temperature. Also, we note that the single-particle residue is not fully converged in the intermediate field range, even at the lowest temperatures.

In the static MF scenario, the two Lifshitz transitions are naturally present. As shown in Fig. 3, the single-particle residue $Z_\uparrow$, calculated from the MF coherence factors at the Fermi energy, displays the expected steplike behavior.

The Lifshitz transition at $B = B_{L2}$ equally marks the transition from heavy to light fermions, which is reflected in the steep increase of Z_σ as the magnetic field is ramped up further; see Fig. 6(b). This is in accordance with the notion of adiabatic continuity to free fermions which is expected in the limit of high magnetic fields, i.e., weak coupling.[48] Based on the $\beta t = 200$ DMFT results, we conclude that a continuous transition from low to high magnetic fields occurs, at least at and above this temperature.

V. BEYOND DMFT

The DCA calculates the k-dependent self-energy $\Sigma_\sigma^{\mathrm{DCA}}(\omega_n,\mathbf{K})$. This leads to the estimate for the residue

$$\left[Z_\sigma^{\mathrm{DCA}}(M(\mathbf{k}_f))\right]^{-1} = \lim_{T\to 0}\left[1 - \frac{\mathrm{Im}\Sigma_\sigma^{\mathrm{DCA}}(\omega_n, M(\mathbf{k}_f))}{\omega_n}\right]_{\omega_n=\pi T}, \quad (15)$$

The map function $M:\mathbf{k}_f \to \mathbf{K}$ maps the Fermi momentum to the matching reciprocal patch.

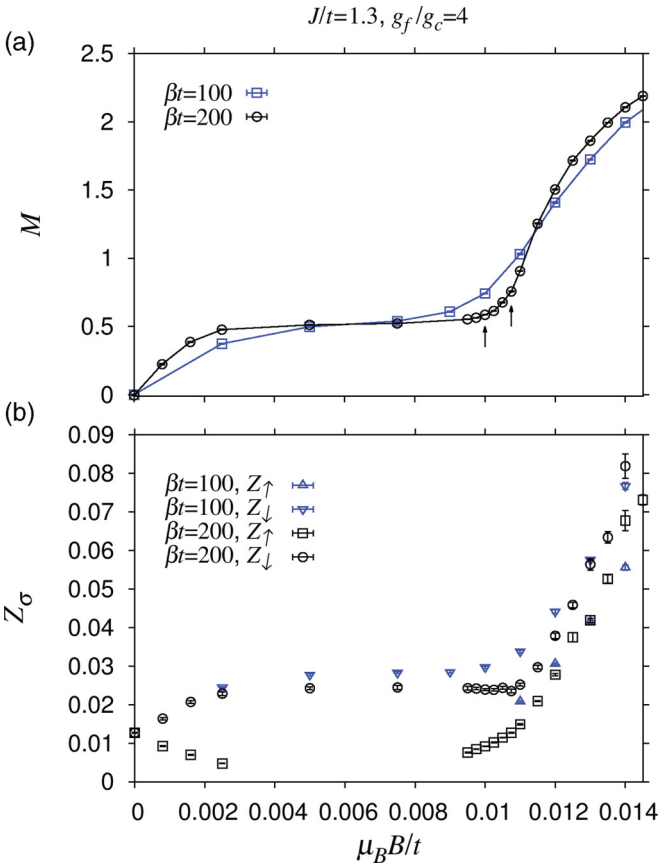

FIG. 6. (Color online) Magnetization M and single-particle residue Z_σ^{DMFT} across the MMT. (The arrows refer to the single-particle spectra of Fig. 5.)

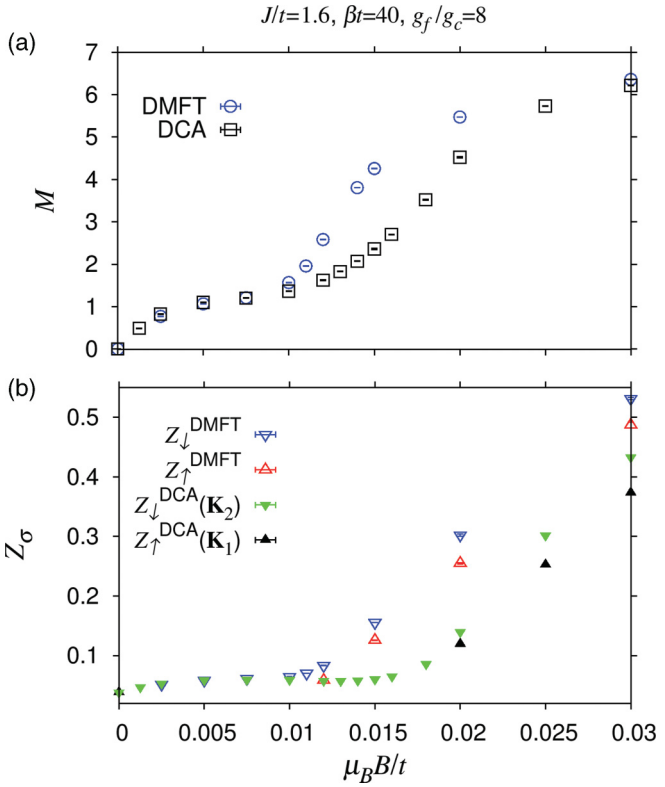

FIG. 7. (Color online) Magnetization M and single-particle residues Z_σ from two-orbital (DMFT) calculations and four-orbital (DCA) calculations. The k vectors $\mathbf{K}_1 = (0,0)$ and $\mathbf{K}_2 = (\pi,\pi)$ denote the relevant DCA patches.

The four-orbital DCA measurements agree with the two-orbital DMFT results in the limits of strong coupling (small magnetic field) and weak coupling (large magnetic fields); see Fig. 7(a). In the intermediate regime, around $B = B_{\mathrm{L2}}$, deviations are detected in the magnetization as well as in the single-particle residues. The inclusion of spatial fluctuations softens the transition considerably. This can be understood from the notion of an effective Landé factor g_f which becomes lower when spatial fluctuations are present, since, on the two-site cluster, the local moment can be quenched not only dynamically but also via local singlet formation. The single-particle residue in the down-spin projection displays no sign of vanishing across the MMT [Fig. 7(b)].

VI. DISCUSSION

Lifshitz transitions are continuous quantum phase transition which do not change symmetry but Fermi surface topology.[21] Strictly speaking, they are defined for free fermion systems at zero temperature. Due to the unambiguous presence of quasiparticles, the notion of Lifshitz transition can be carried over to the KLM. Driven by the external magnetic field, two consecutive Lifshitz transitions take place, at $B = B_{\mathrm{L1,2}}$, and the second one is identified with the MMT. This scenario is maintained when the f moments are allowed to couple more strongly to the field by altering the ratio g_f/g_c.

Collective effects challenging the quasiparticle coherence seem to be of minor importance during the MMT, even when $B \sim T_{\mathrm{coh}}$. Naturally, our calculation scheme is limited to the dominantly paramagnetic regime of the KLM. The choice of parameters $n_c = 0.9$ and $J/t \geqslant 1.3$ places our results unambiguously in the paramagnetic phase.[32,35,36] First steps (Fig. 7) in a systematic DCA study of larger clusters that can take into account the Ruderman-Kittel-Kasuya-Yosida (RKKY) interaction between local moments leave the Lifshitz scenario at the MMT invariant. This is consistent with the fact that temporal fluctuations that generate the Kondo effect dominate the physics at the MMT. Close to a critical point where the range of spatial fluctuations becomes large our approximation will fail and another modeling will be required.

Transport signatures of the Lifshitz transition can be calculated with the Boltzmann transport approximation. Topological changes of the bands that cross the Fermi energy can strongly influence transport measurements, in particular when these bands are shallow. This offers an explanation for the anomalies observed in Zeeman driven heavy-fermion systems.[26]

Compared to our results for the magnetic field dependent single-particle spectrum (Fig. 5), similar results have been obtained for the ferromagnetic phase of the Kondo lattice model without external field terms.[49] There, the spin-dependent shift of the quasiparticle weight is generated dynamically and leads to the notion of a spin-selective Kondo insulating phase.

Our results are applicable to heavy fermion compounds that have a magnetic-field-driven Lifshitz transition at the coherence scale.

The materials CeTiGe[5] and $CeRu_2Si_2$[6,50] have a MMT at magnetic energy scales that are consistent with their estimated coherence temperatures. In our model, the critical metamagnetic field corresponds to the second Lifshitz transition at B_{L2}. In this mechanism of competing energy scales we expect that the details of the band structure are of secondary importance. This is in contrast to Lifshitz transitions at magnetic fields much below the coherence scale where the details of the band structure are essential.[26]

The metamagnetic signatures of our model (Fig. 1) are similar to recent experimental data of the paramagnetic $4f$-based compound CeTiGe, which exhibits a pronounced first-order MMT.[5] Its anticipated coherence scale, $T_{\mathrm{coh}} \approx 55$ K, is of the same order as the critical magnetic field of $\mu_0 B_{\mathrm{MMT}} = 12.5$ T, assuming in our model a g factor $g_f \approx 7$. Equally, at lower fields, the magnetization is found to slightly change its slope, which might correspond to a first Lifshitz transition which in our model happens at B_{L1}. The experimentally observed distinct drop of the effective quasiparticle mass is in accordance with our findings for the KLM (see Sec. IV). Importantly, we find the MMT to be continuous both in the two-orbital DMFT and in the four-orbital DCA calculations and on the temperature scales we can access.

$CeRu_2Si_2$ exhibits a continuous MMT and simultaneously a Zeeman-driven topology change of the Fermi surface.[6,7] The magnetization increases seemingly linear as the magnetic field is increased towards the metamagnetic field.[50] The critical field $\mu_0 B_{\mathrm{MMT}} = 7.8$ T matches the coherence temperature of $T_{\mathrm{coh}} \approx 20$ K[6,50] when the g factor in our model is assumed to be $g_f \approx 4$. A Lifshitz transition at the coherence scale is therefore a plausible scenario for the MMT in $CeRu_2Si_2$.

VII. CONCLUSION

We have explored the Zeeman driven MMT in the Kondo lattice model which is considered to be the paradigmatic low-energy model for heavy fermion systems. Results for the paramagnetic metallic phase of the KLM are obtained in the framework of DMFT/DCA, which can exactly account for the Kondo effect.

Upon scaling the relevant energy scales with the lattice coherence scale, the collapse of the magnetization data to a universal curve is observed, independent of the Kondo interaction. This data collapse has been confirmed for a range of Kondo couplings, temperatures, and ratios of Landé factors. The pseudospin nature of the f orbitals, resulting from a Kramer's doublet, can be taken in account with an effective Landé factor g_f and the competition of magnetic scale and coherence scale is invariant on the choice of g_f.

We have traced the single-particle residue from low to high magnetic fields and report that it is continuous at the lowest temperatures our simulation can access. Two consecutive Lifshitz transitions occur as the field is ramped up and cause the change in topology of the spin-projected Fermi surfaces. This lead us to the finding that the MMT in the KLM is coincident with a continuous Lifshitz transition. The absence of a singularity in the single-particle residue at the MMT excludes the Kondo breakdown scenario.

At the temperature scale we can access, the sharp increase of magnetization at the MMT can well be explained as a consequence of a continuous Lifshitz transition in heavy-fermion model systems where the Landé factor of the local spins is larger than the one for the itinerant electrons. In the course of this transition the excitations change their character from heavy fermions to light fermions.

The recently observed first-order nature[5] of the metamagnetic phase transition at a temperature $T \ll T_{\mathrm{coh}}$ remains an open issue. Of particular importance is understanding if the KLM itself can account for the low-temperature first-order nature of the transition or if other competing energy scales such as coupling to the lattice[51] have to be taken into consideration.

ACKNOWLEDGMENTS

We would like to thank A. Benlagra, M. Brando, and H. Pfau for discussions and F. Goth for a careful reading of the manuscript. We acknowledge support from the DFG under Grant No. FOR1162. The numerical simulations were carried out at the Jülich Supercomputing Centre and we thank this institution for generous allocation of CPU time.

[1] P. Gegenwart, Q. Si, and F. Steglich, Nature Phys. **4**, 186 (2008).
[2] S. Yamamoto and Q. Si, J. Low Temp. Phys. **161**, 233 (2010).
[3] P. Coleman and A. Nevidomskyy, J. Low Temp. Phys. **161**, 182 (2010).
[4] P. Haen, J. Flouquet, F. Lapierre, P. Lejay, and G. Remenyi, J. Low Temp. Phys. **67**, 391 (1987).
[5] M. Deppe, S. Lausberg, F. Weickert, M. Brando, Y. Skourski, N. Caroca-Canales, C. Geibel, and F. Steglich, Phys. Rev. B **85**, 060401 (2012).
[6] R. Daou, C. Bergemann, and S. R. Julian, Phys. Rev. Lett. **96**, 026401 (2006).
[7] H. Pfau, R. Daou, M. Brando, and F. Steglich, Phys. Rev. B **85**, 035127 (2012).
[8] H. Aoki, S. Uji, A. K. Albessard, and Y. Onuki, Phys. Rev. Lett. **71**, 2110 (1993).
[9] M. Sugi, Y. Matsumoto, N. Kimura, T. Komatsubara, H. Aoki, T. Terashima, and S. Uji, Phys. Rev. Lett. **101**, 056401 (2008).
[10] S. Kitagawa, H. Ikeda, Y. Nakai, T. Hattori, K. Ishida, Y. Kamihara, M. Hirano, and H. Hosono, Phys. Rev. Lett. **107**, 277002 (2011).
[11] W. Wu, A. McCollam, S. A. Grigera, R. S. Perry, A. P. Mackenzie, and S. R. Julian, Phys. Rev. B **83**, 045106 (2011).
[12] F. Weickert, M. Brando, F. Steglich, P. Gegenwart, and M. Garst, Phys. Rev. B **81**, 134438 (2010).
[13] A. J. Millis, A. J. Schofield, G. G. Lonzarich, and S. A. Grigera, Phys. Rev. Lett. **88**, 217204 (2002).

[14]S. Viola Kusminskiy, K. S. D. Beach, A. H. Castro Neto, and D. K. Campbell, Phys. Rev. B **77**, 094419 (2008).
[15]O. Howczak and J. Spałek, J. Phys.: Condens. Matter **24**, 205602 (2012).
[16]K. S. D. Beach and F. F. Assaad, Phys. Rev. B **77**, 205123 (2008).
[17]T. Yamada and Y. Ōno, J. Phys. Soc. Jpn. **80SA**, SA131 (2011).
[18]B. Binz and M. Sigrist, Europhys. Lett. **65**, 816 (2004).
[19]C. Honerkamp, Phys. Rev. B **72**, 115103 (2005).
[20]E. Bauer and M. Rotter, in *Properties and Applications of Complex Intermetallics*, edited by E. Belin-Ferrero (World Scientific, Singapore, 2009), Chap. 5, pp. 183–248.
[21]I. M. Lifshitz, Sov. Phys. JETP **11**, 1130 (1960).
[22]Y. Blanter, M. Kaganov, A. Pantsulaya, and A. Varlamov, Phys. Rep. **245**, 159 (1994).
[23]Y. Yamaji, T. Misawa, and M. Imada, J. Phys. Soc. Jpn. **75**, 094719 (2006).
[24]G.-M. Zhang, Y.-H. Su, and L. Yu, Phys. Rev. B **83**, 033102 (2011).
[25]A. Hackl and M. Vojta, Phys. Rev. B **77**, 134439 (2008).
[26]A. Hackl and M. Vojta, Phys. Rev. Lett. **106**, 137002 (2011).
[27]A. C. Hewson, *The Kondo Problem To Heavy Fermions* (Cambridge University Press, Cambridge, UK, 1997).
[28]O. Bodensiek, R. Zitko, R. Peters, and T. Pruschke, J. Phys.: Condens. Matter **23**, 094212 (2011).
[29]J. R. Schrieffer and P. A. Wolff, Phys. Rev. **149**, 491 (1966).
[30]H. Tsunetsugu, M. Sigrist, and K. Ueda, Rev. Mod. Phys. **69**, 809 (1997).
[31]H. Tsunetsugu, Phys. Rev. B **55**, 3042 (1997).
[32]J. Otsuki, H. Kusunose, and Y. Kuramoto, Phys. Rev. Lett. **102**, 017202 (2009).
[33]M. H. Hettler, M. Mukherjee, M. Jarrell, and H. R. Krishnamurthy, Phys. Rev. B **61**, 12739 (2000).
[34]M. Jarrell, T. Maier, C. Huscroft, and S. Moukouri, Phys. Rev. B **64**, 195130 (2001).
[35]H. Watanabe and M. Ogata, Phys. Rev. Lett. **99**, 136401 (2007).
[36]L. C. Martin, M. Bercx, and F. F. Assaad, Phys. Rev. B **82**, 245105 (2010).
[37]F. F. Assaad, Phys. Rev. B **70**, 020402 (2004).
[38]S. Burdin, A. Georges, and D. R. Grempel, Phys. Rev. Lett. **85**, 1048 (2000).
[39]M. Klein, A. Nuber, H. Schwab, C. Albers, N. Tobita, M. Higashiguchi, J. Jiang, S. Fukuda, K. Tanaka, K. Shimada, M. Mulazzi, F. F. Assaad, and F. Reinert, Phys. Rev. Lett. **106**, 186407 (2011).
[40]C. Praetorius, A. Koehl, B. Muenzing, H. Bardenhagen, and K. Fauth (2012), arXiv:1203.5272 [cond-mat.str-el].
[41]S. Burdin, in *Properties and Applications of Thermoelectric Materials*, NATO Science for Peace and Security Series B: Physics and Biophysics, edited by V. Zlati and A. C. Hewson (Springer, Amsterdam, 2009), pp. 325–340.
[42]D. Withoff and E. Fradkin, Phys. Rev. B **34**, 8172 (1986).
[43]S. Capponi and F. F. Assaad, Phys. Rev. B **63**, 155114 (2001).
[44]S. Saremi and P. A. Lee, Phys. Rev. B **75**, 165110 (2007).
[45]F. F. Assaad and H. G. Evertz, *Computational Many-Particle Physics*, edited by H. Fehske, R. Schneider, and A. Weiße, Vol. 739 (Springer, Heidelberg, 2008) Chap. 10.
[46]D. Tanasković, K. Haule, G. Kotliar, and V. Dobrosavljević, Phys. Rev. B **84**, 115105 (2011).
[47]K. S. D. Beach, eprint arXiv:cond-mat/0403055 (2004).
[48]A. Benlagra, T. Pruschke, and M. Vojta, Phys. Rev. B **84**, 195141 (2011).
[49]R. Peters, N. Kawakami, and T. Pruschke, Phys. Rev. Lett. **108**, 086402 (2012).
[50]J. Flouquet, P. Haen, S. Raymond, D. Aoki, and G. Knebel, Physica B: Condens. Matter **319**, 251 (2002).
[51]M. Raczkowski, P. Zhang, F. F. Assaad, T. Pruschke, and M. Jarrell, Phys. Rev. B **81**, 054444 (2010).